Climate Dynamics (2004) 23: 407–425
DOI 10.1007/s00382-004-0441-x

T. G. D. Casal · J. E. Kutzbach · L. G. Thompson

Present And Past Ice-Sheet Mass Balance Simulations For Greenland And The Tibetan Plateau

Received: 25 July 2003 / Accepted: 15 April 2004 / Published online: 29 July 2004

Abstract Net annual mass balance was evaluated for Greenland and the Tibetan Plateau using the meteorological forcings from the NCEP reanalysis and two GCMs (FOAM1.0 and CSM1.4) for modern climate and for different time periods extending back to the beginning of the Holocene (11,000 years ago) for the climate models. The ice-sheet budget calculations, using the degree day methodology, were performed on a finer grid than the model output by interpolating monthly precipitation and surface temperature and correcting the latter to account for the GCM's smoothed topography. The computed net mass balance for Greenland in the present day is positive and it ranges between 290–300 mm water equivalent (w.e.)/year for the two models, values close to the NCEP estimate of 250 mm/year. The past climate simulations show that the Greenland mass balance has become slightly more positive since the beginning of the Holocene. The Tibetan Plateau's present-day area average net mass balance is negative and ranges between –1200 and –2000 mm w.e. /year for the two models, values bracketing the NCEP estimate of 1700 mm/year, although the balance is positive over small regions of the plateau consistent with the existence of small ice caps and glaciers. The calculated past mass balance shows an increasingly less negative value for FOAM from 11,000 years ago towards the present and expansion of the positive mass balance areas, mainly due to decreased snow ablation as the summertime insolation decreases with the changes in orbital forcing; in CSM the opposite trend occurs but changes are smaller and less systematic. The result from FOAM shows that the likelihood of ice sheets developing on the Tibetan Plateau may have increased since 11000 years ago, which is consistent with some glacial records.

T. G. D. Casal (✉)
Now at the Rosenstiel School of Marine
and Atmospheric Sciences, University of Miami,
4600 Rickenbacker Cswy, Miami,
FL 33149-1098, USA
E-mail: tcasal@rsmas.miami.edu

J. E. Kutzbach
Center for Climatic Research and Department Atmospheric,
Oceanic Science University of Wisconsin-Madison, USA

L. G. Thompson
Byrd Polar Research Center,
Ohio State University, OH, USA

1 Introduction

The changes in mass balance of ice sheets are an important component of Earth's changing climate. The growth and wasting of ice sheets are commonly cited indices of global climate change, both directly and for the associated impact on global sea-level. In the past, the growth and decay of ice sheets have marked the onset and termination of glaciations (Imbrie and Imbrie 1979). At present, earth scientists assess observations (satellite and sea-level) and ice-sheet mass balance estimates for current trends (Ohmura and Reeh 1991; Van de Wal 1996; Abdalati and Steffen 1997; Stroeve et al. 1997) and examine simulations of future climates for estimating future ice-sheet mass balance scenarios (IPCC 2001; Van de Wal et al. 2001; Ohmura et al. 1996; Wild et al. 2003).

However, estimating mass balance is difficult using either observations or models. With observations, there are problems associated with the lack of direct measurements over the ice sheets. With model simulations, there is a recognition that the low resolution of climate models implies that the elevations of mountains and plateaus are too low, and this error in specifying topography leads to biases in the model's simulation of temperature and precipitation. Various schemes have been proposed to correct for these biases.

In spite of these difficulties, observational evidence of the presence or absence of ice sheets, both at present and in the past, provides some basic information on the planet's ice sheets that can be compared with these estimates of mass balance from models. In this work we

focus particular attention on two regions. We use the region of the Greenland Ice Sheet to compare present-day observations and simulations of ice-sheet mass balance. We use the region of the Tibetan Plateau to examine both present-day circumstances (several small ice sheets) and evidence of changes in these ice sheets over the last 11,000 years. Presence or absence of large ice sheets on the Tibetan Plateau, or even longer-than-average springtime snow cover, is thought to influence the strength of the Asian monsoon, and hence the history and potential future of ice on the Tibetan Plateau is an important topic.

The purpose of this work is twofold: (1) to assess the accuracy of observations and low-resolution climate models for estimating present-day ice sheet mass balance for the regions of Greenland and the Tibetan Plateau, and (2) to assess possible changes in mass balance in the Holocene (approximately the past 10,000 years) of ice sheets on the Tibetan Plateau using paleoclimate simulations. It will be shown that, with appropriate corrections, the modern-day NCEP data sets give satisfactory estimates of ice-sheet mass balance for both Greenland and the Tibetan Plateau. It will also be shown that appropriately corrected data sets from two climate models, FOAM1.0 and CSM.1.4, provide reasonable estimates of modern day ice-sheet mass balances for Greenland and the Tibetan Plateau, and that the trend in simulated ice-sheet mass balance for the Tibetan Plateau in the Holocene, particularly from one of the two models, agrees with some observational records from ice cores.

Section 2 contains a literature review of previous studies and techniques for mass balance studies. Section 3 describes the observations and model simulations used in the analysis. Section 4 presents ice-sheet mass balance results for Greenland, while Sect. 5 presents the results for the Tibetan Plateau. Conclusions and suggestions for additional work are in Sect. 6.

2 Previous studies of ice-sheet mass balance

In this section, a description of previous ice sheet mass balance studies for Greenland and the Tibetan Plateau is presented, including: (2.1) an overview, (2.2) a description of the technique of Marshall et al. (2002) for correcting mass balance calculations for elevations bias; (2.3) and (2.4) are a survey of papers describing observations and simulations of present and past ice sheets as well as estimates of mass balances.

2.1 Methods for estimating ice sheet mass balance

Van de Wal (1996) compared the performance of a degree day model and an energy-balance model for the Greenland ice-sheet mass balance. Energy balance models require knowledge of atmospheric variables (such as atmospheric humidity and longwave radiation) which are usually poorly known or poorly modeled at the fine scale of glaciers while the degree day models rely on temperature index methods. The input for both models was elevation, latitude and accumulation; both models calculated the annual ablation. The results were compared with the available mass balance measurements. The results were very similar for both models but regional discrepancies occurred, particularly in northern Greenland. The energy balance model predicted a more accurate mass balance gradient with elevation and was less sensitive to temperature perturbations than the degree day model.

Braithwaite (1996) also compared the two models performance in calculating melting and refreezing in discrete locations of the Greenland ice sheet (most of them located in West Greenland) and found that the energy balance model was more realistic but required input data that were not available over the entire ice sheet while the parameters used in the degree day model varied from one situation to another. Marshall et al. (2002) reconstructed North America's ice sheets during the Last Glacial Maximum (LGM) in order to quantify the uncertainty associated with glaciological reconstructions, such as ice sheet thickness and volume; the ice sheet mass balance was parametrized using the degree day methodology.

Because the two methods give roughly equivalent results, we will use the degree day method because of its greater simplicity in relying entirely on temperature corrections.

2.2 The mass balance calculations using the degree day technique

Our calculation of the ice-sheet mass balances in Greenland and the Tibetan Plateau follows the degree day approach described in Marshall et al. (2002) and Marshall and Clarke (1999). The approach calculates accumulation, ablation and net mass balance (accumulation minus ablation). A degree-day model is used to partition monthly precipitation into rain and snow fractions (using T = 1 °C as a threshold). Ablation is also calculated as a function of degree days (using T = 0 °C as a threshold), with parameters representing melt factors being used to convert degree day totals to ablation. The degree day melt factor used for snow (d_{snow}) was 3 mm year^{-1} °C^{-1} and for ice (d_{ice}) was 8 mm year^{-1}° C^{-1}. A correction for the refreezing of meltwater was applied using the factor 0.6. (Marshall et al. 2002).

All the parameters used in these calculations were developed for Greenland. It is not at all clear that the melt rates parameters, d_{snow} and d_{ice} should be extrapolated to lower latitudes where summer insolation is much more intense (Marshall et al. 2002); however, due to the lack of observations for the Tibetan Plateau, the same values were used in this study for the mass balance calculations for the Tibetan Plateau. In future work, it

would be desirable to consider any necessary adjustments to the approach.

2.3 Simulations and observations of ice-sheet mass balance for Greenland, for the past and future

Observations compiled by Ohmura and Reeh (1997) yielded two maps of annual total precipitation and accumulation for Greenland. They concluded that topography was very important in determining the regional accumulation on the ice sheet and estimated that the total mean accumulation rate in Greenland is 310 mm water equivalent (w.e.) per year. Maximum accumulation of 1500 mm w.e. occurs in the southeastern corner of Greenland and minimum values of less than 100 mm w.e. are found in the northeast slope of the ice sheet.

Thompson and Pollard (1997) calculated the Greenland and Antarctic mass balances for the present and doubled atmospheric CO_2 using the GENESIS Version-2 Global Climate Model. Corrections were applied to the lowest level AGCM meteorological fields to improve their ice-sheet estimates because their AGCM topography was lower than most Greenland elevations and the refreezing of meltwater was included. Variables such as surface temperature were lowered by a constant lapse rate multiplied by the difference between the true elevation and the AGCM elevation. They found a value of 130 mm/year for present-day net annual surface mass balance on Greenland and concluded that it would decrease to –120 mm/year under doubled CO_2 conditions. In a similar study but using observational data, Huybrechts et al. (1991) studied the sensitivity of Greenland's ice mass budget to a greenhouse warming and they concluded that rising temperatures increased runoff and accumulation but since the later exceeded the former, a total mass balance reduction in the ice sheet would be expected. Van de Wal et al. (2001) and Wild et al. (2003) confirmed the previous results.

Finally, Pollard and PMIP Participating Groups (2000) computed ice-sheet surface mass budgets using the meteorological forcings from 17 different GCMs for the present, 6000 and 21,000 calendar years before present in Greenland, as well as Antarctica and the Laurentide and Eurasia ice sheets at the Last Glacial maximum (LGM), to assess how well the simulated mass balances agreed with each other. All 17 GCM's meteorological fields were interpolated to a finer grid, where corrections were applied to account for the GCM's topographic biases, and were driven by a common snow/ice surface model. The results showed that large climatic differences between the models, mainly due to the several degrees differences in summer surface air temperatures in the studied regions, caused considerable scatter in the computed ice sheet budgets with the exception of Antarctica. However, using a Delta method, the results were quite consistent for 6 k, showing higher ablation values compared to the present.

2.4 Observational studies of changes in ice sheets on the Tibetan Plateau, during the Holocene

The Tibetan Plateau is a massive elevated land mass that spans an area of 2.5×10^6 Km^2 with an average elevation of 4.5 Km. Glaciers are found in various regions of the plateau (Thompson et al. 1997). We will mention several of these glaciers.

The Guliya ice cap is located in northwest region of the plateau, and covers an area around 200 km^2 with a summit elevation of 6710 m above sea level. Its average annual accumulation is in the order of 200 mm w.e. (Thompson et al. 1997). It is believed that the Guliya ice cap records cover more than 100,000 years (Christner et al. 2003). In the northeastern region, the Dunde ice cap covers 60 km^2, lies at an elevation of 5325 m, and is 140 m thick. It accumulates annually around 400 mm w.e. and it, too, may be more than 100,000 years old (Thompson et al. 1989). Pollen records from Dunde suggest that the summer monsoon extended further north and west than today between 10,000 to 4800 year B.P due to orbital forcing alone, and retreated during the middle Holocene (Liu et al. 1998).

The Dasuopu glacier is located in the southwestern region of the Tibetan Plateau and is a high elevation site (7200 m). The calculations of the average annual net balance yield a value around 1000 mm w.e. (Thompson et al. 2000) and interestingly, it is likely that the Dasuopu ice cap began to accumulate in the Holocene, between 6000 to 8000 years BP. Moreover, recent and continuing work in Central Tibet on the Puruogangri ice cap also suggests accumulation beginning in the Holocene (Lonnie Thompson work in progress).

The details of the climatic factors involved in the seasonal mass balances of these glaciers is still poorly known, although it is likely that the northern sites are influenced by both summer monsoon precipitation and winter (westerly) precipitation coming from the Atlantic and the Mediterranean, whereas the southern and central sites, where ice seems to have developed during the Holocene, may be primarily influenced by the summer monsoon. Our simulations of past climates of the Holocene will provide estimates of possible changes in ice-sheet mass balance that can be compared to these observations (Lonnie Thompson work in progress).

3 Description of the datasets and comparisons between the simulations and observations

In this section, we describe the datasets and models and assess the general performance of the models.

3.1 Description of the datasets and paleo simulations

The observational/model NCEP Reanalysis data was provided by the NOAA-CIRES Climate Diagnostics Center, Boulder, Colorado, USA, from their Web site at

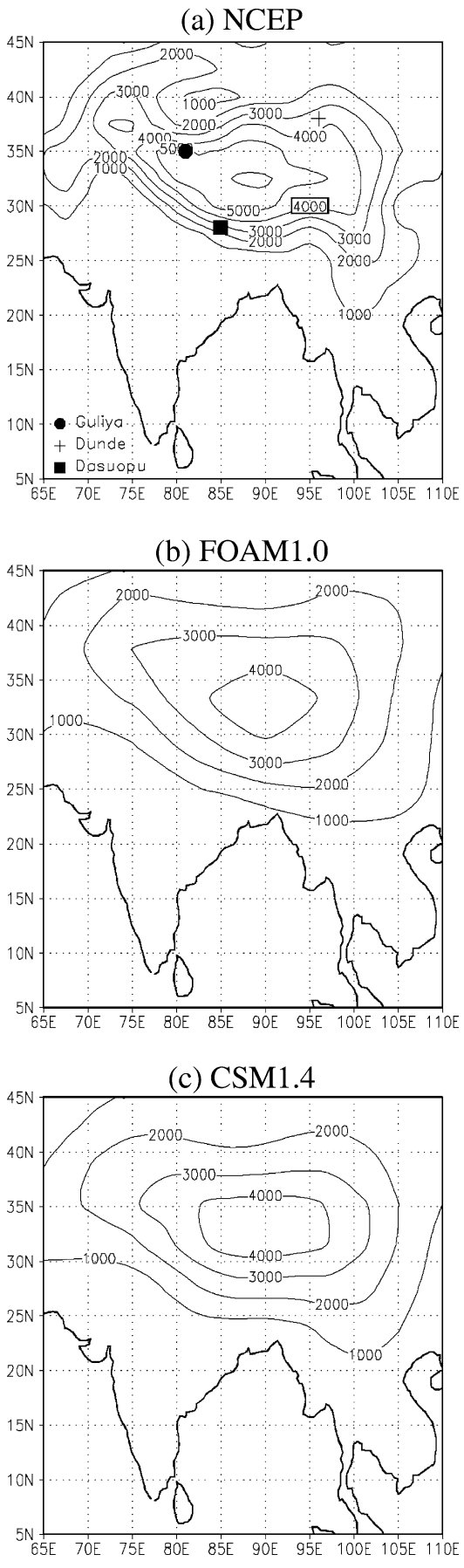

Fig. 1 Topography for the Tibetan Plateau (in m): **a** NCEP, with the location of the Dunde, Dasuopu and Guliya ice caps, **b** FOAM1.0 and **c** CSM1.4

http://www.cdc.noaa.gov/. The temperature data consists of monthly long term means on a 2.5° × 2.5° latitude/longitude grid and the precipitation data consists of daily precipitation rate in a 1.914° latitude × 1.875° longitude grid which was then converted to monthly long-term means.

One set of the GCM data is from version 1.0 of FOAM, which is a fully coupled ocean-atmosphere model (Jacob 1997) without flux adjustment. The atmospheric component is a parallel version of the NCAR CCM2 with a spectral resolution of R15 (equivalent to 7.5° longitude × 4.4° latitude) and 18 levels, with the atmospheric physics replaced by those of CCM3. The oceanic component is similar to the GFDL MOM, the land surface model is nearly identical to the default land surface model of CCM2 (but including a prognostic box hydrology model from CCM1) and it incorporates a simple thermodynamic sea-ice model. Starting from the 600th year of a long modern control run, all coupled simulations were integrated for 150 years; this relatively short integration is a potential limitation on our conclusions since the deep ocean takes longer to reach equilibrium. Since the atmosphere and upper ocean reached quasi-equilibrium in the first decades (it drifted only in the first 30 years), the last 120 years were used to construct the monthly climatology. Climates were simulated under the insolation forcings of the present day or control run (0 k), 3000 years ago (3 k), 6000 years ago (6 k), 8000 years ago (8 k) and 11,000 years ago (11 k). The dominant insolation forcing in the early to mid Holocene is an increased seasonal cycle in the NH and a decreased seasonal cycle in the SH. Consequently, there is a decrease in maximum summer insolation towards the present in the NH (from 477 W/m^2 in July at 11 k to 448 W/m^2 in July for 0 k) and an opposite trend in the SH (Liu et al. 2004).The atmospheric concentration of $C0_2$ was prescribed at 330 ppmv in all experiments.

Version 1.4 of CSM was also used for present-day and Holocene climate simulations. CSM1.4 is a coupled model, without flux adjustment (Shin et al. 2003). It consists of four independent components representing the atmosphere, ocean, land surface and sea-ice that communicate with each other through a flux coupler. The atmospheric component is the Community Climate model, CCM (Kiehl et al. 1998) version 3.6 with a spectrally truncated T31 horizontal grid resolution

Fig. 2 Simulated monthly water equivalent snow depth, **a, b** in mm water equivalent, w.e, **c, d** precipitation in mm/month and **e, f** surface temperature in ° C for the grid square nearest to the Dunde ice cap location (see *small map inset* in precipitation panel) for FOAM1.0 (*left panels*) and CSM1.4 (*right panels*). The simulations are for 0 k (*dots*), 6 k (*squares*) and 11 k (*crosses*)

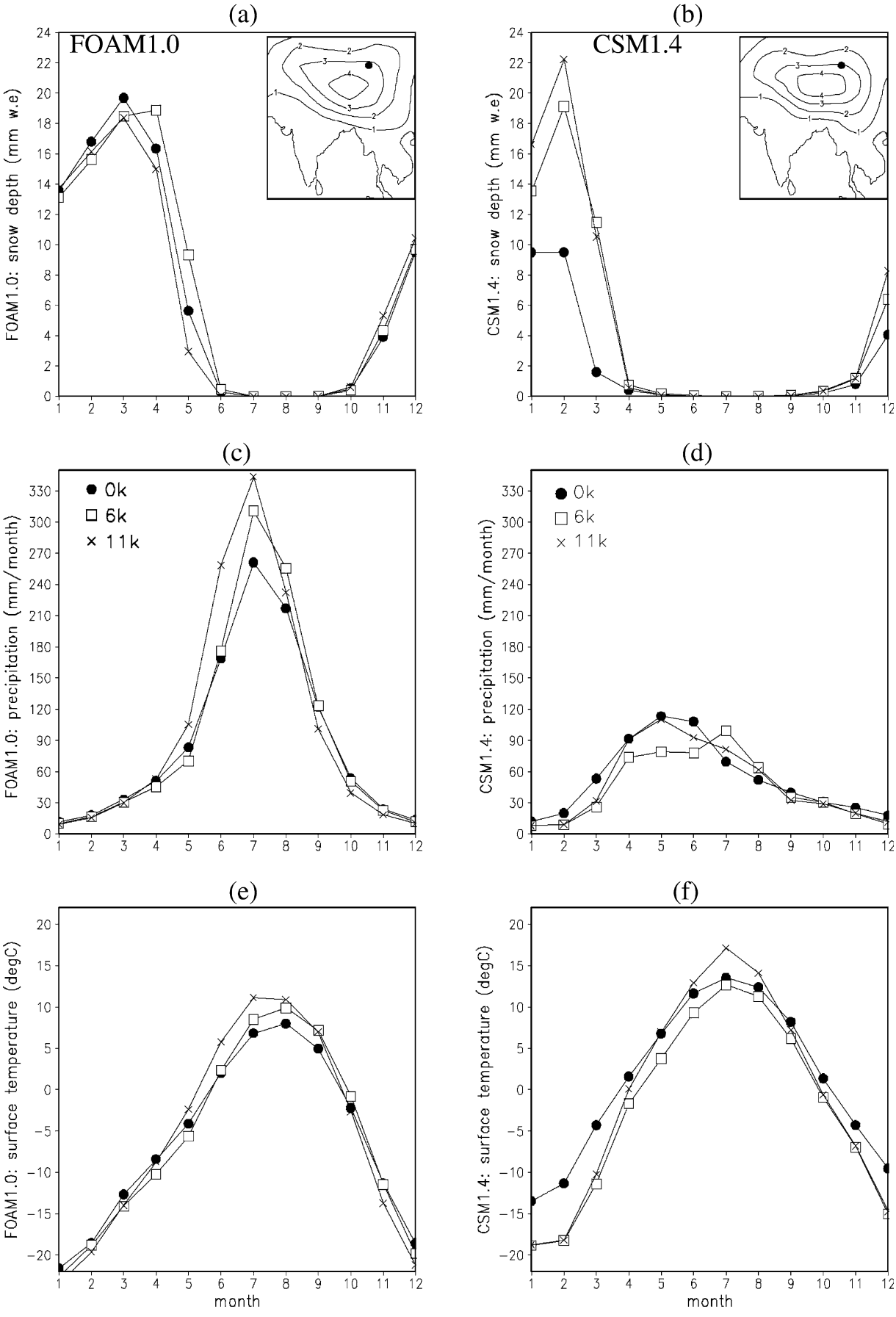
(a)
FOAM1.0
FOAM1.0: snow depth (mm w.e)
(b)
CSM1.4
CSM1.4: snow depth (mm w.e)
(c)
0k
6k
11k
FOAM1.0: precipitation (mm/month)
(d)
0k
6k
11k
CSM1.4: precipitation (mm/month)
(e)
FOAM1.0: surface temperature (degC)
month
(f)
CSM1.4: surface temperature (degC)
month

($\backsim 3.75°$ in latitude and longitude) and 18 vertical levels. The ocean component is the NCAR-CCSM Ocean Model (NCOM; Gent et al. 1998). The CSM experiments were integrated for 100 years and the last 50 years were used to construct the monthly climatology. The insolation forcings for the simulated Holocene climates were set at 0 k, 6 k and 11 k for the respective runs (insolation values are very similar to those of FOAM1.0) and the CO_2 concentration was set to the pre-industrial value of 280 ppmv.

One of the limitations of the experiments with both models is that all experiments have the same prescribed

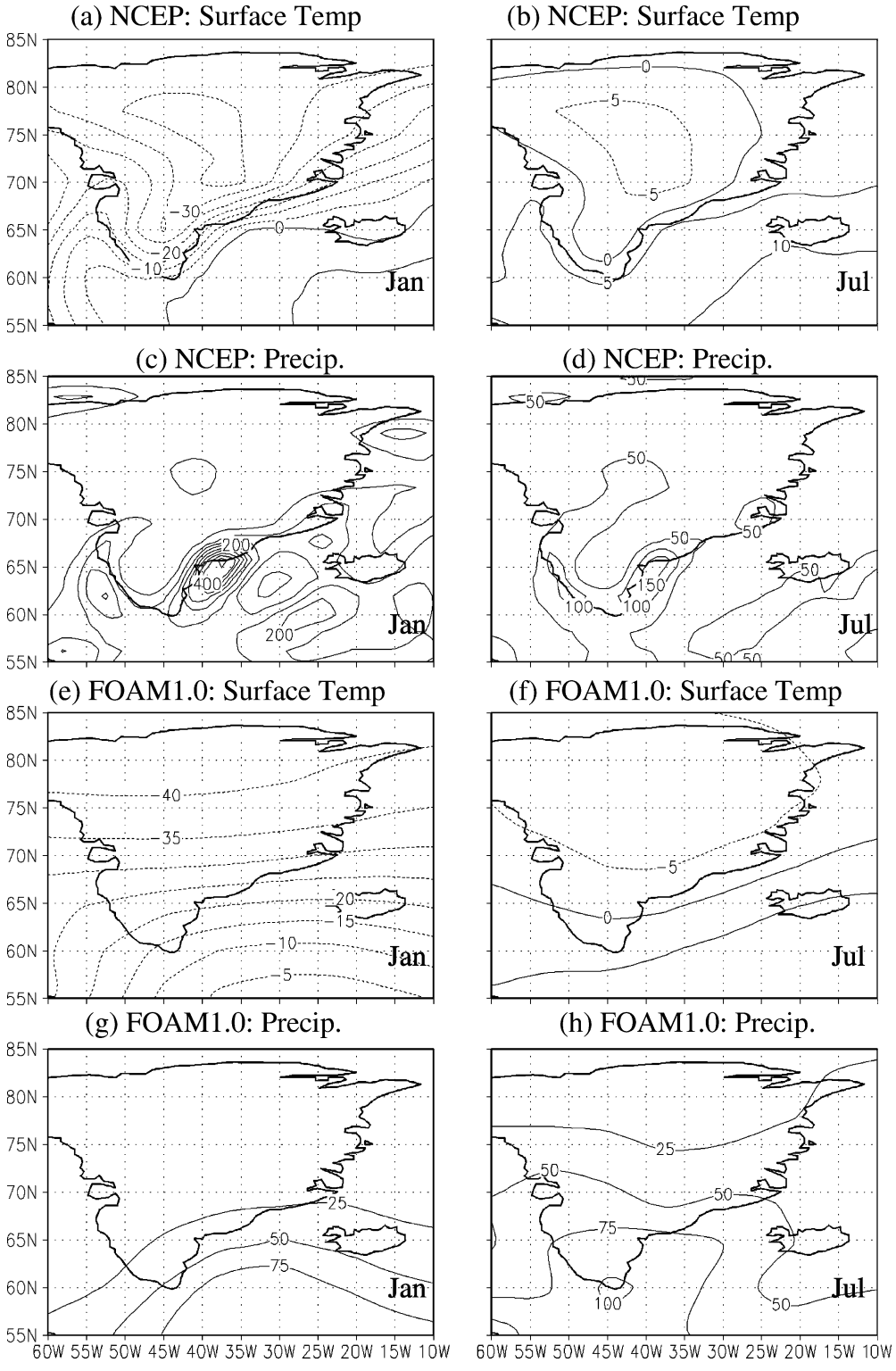

Fig. 3 January and July present-day surface temperature (in °C) **a, b** for NCEP and **e, f** FOAM1.0 as well as precipitation (in mm) **c, d** for NCEP and **g, h** FOAM1.0 for Greenland. *Contour interval* is 5 °C for surface temperature, 50 mm for NCEP's precipitation and 25 mm for FOAM's

Table 1 Area average surface temperature (in °C) and monthly cumulative precipitation (in mm) for present day Greenland, for NCEP, FOAM1.0 and CSM1.4. The area average was calculated for every grid point on land

0 k	Surface temperature(°C)			Monthly cumulative precipitation(mm)		
	January	July	Annual	January	July	Annual
NCEP	–32.0	1.1	–11.7	22.9	42.4	57.5
FOAM1.0	–35.2	–5.3	–20.7	10.5	39.1	26.8
CSM1.4	–22.8	–0.1	–12.4	40.1	44.4	41.8

continental ice sheet, land vegetation cover and CO_2 concentrations as found in their respective control runs (Liu et al. 2003), and therefore they did not include the North American and European ice sheets which were still relatively extensive at 11 k and did not disappear entirely until after 8 k. Therefore, these sensitivity experiments only investigate the changes in mass balance due to orbital forcing, which was a dominant climate forcing in the Holocene, but not the only source of possible altered forcing. We note also that the different levels of CO_2 concentration in the two models (280 and 330 ppmv, respectively) represents another cause of possible differences in base state climate but should have a relatively minor influence on the assessment of the sensitivity of the simulations to changed orbital forcing.

3.2 First assessment on the performance of the two GCM models

As previously mentioned, one difficulty in simulating ice-sheet mass balances in GCM's is the models' inability, owing to coarse spectral resolution, to reproduce topographic features accurately (Thompson et al. 1997). This problem is exemplified in Fig. 1, which shows that the Tibetan Plateau topography for NCEP (Fig. 1a) is more accurate and more detailed than is the topography of FOAM1.0 or CSM1.4 (Fig. 1b,c), due to the lower resolution of the climate models.

In order to illustrate the general accuracy of the two models, FOAM1.0 and CSM1.4, in one region, snow depth as well as precipitation and surface temperature were examined for the Tibetan Plateau. Figure 2 illustrates the seasonal results for the grid square corresponding most closely to the region of the Dunde ice cap location, for FOAM1.0 and CSM1.4. In both models, all the snow that accumulates in the winter, melts in the summer time (Fig. 2a, b), therefore the existence of an ice sheet is not possible; however, in this calculation temperature was not corrected to account for the topographic bias (a correction included in subsequent calculations). Note that the surface temperature (Fig. 2e, f) in both models is above freezing during the entire summer, for all three cases. This is what Thompson and Pollard (1997) found in their model results because of the elevation truncation in the model and it shows that a temperature correction is necessary in order to yield reliable ice-sheet mass balance results. Precipitation peaks in the summer for FOAM1.0 in all three cases (Fig. 2c), which agrees with known observations that the accumulation season and melting season in the Tibetan Plateau coincide (Liu et al. 1998). The precipitation for CSM1.4 (Fig. 2d) does not show as large a peak in the wet season. The results for the Guliya and Dasuopu ice caps, for both models (not shown) are very similar to Dunde's for snow depth and surface temperature, but they do not show the precipitation maximum in the summer.

4 Mass balance calculations for Greenland

Since the mass balance of Greenland is fairly well studied, at least relative to that of the Tibetan Plateau, we use the Greenland results to help assess the accuracy of the model. In the following section the results for Greenland will be analyzed.

Table 2 Same as Table 1, for Greenland, except for past climate simulations from FOAM1.0 and CSM1.4.

FOAM1.0	Surface temperature(°C)			Monthly cumulative precipitation(mm)		
	January	July	Annual	January	July	Annual
0 k	–35.2	–5.3	–20.7	10.5	39.1	26.8
3 k	–35.5	–6.1	–21.7	11.2	35.8	26.2
6 k	–32.3	–3.1	–18.3	12.7	41.7	29.9
8 k	–32.8	–2.5	–18.3	12.1	42.0	29.7
11 k	–33.0	–1.7	–18.0	11.7	46.1	30.5
CSM1.4						
0 k	–22.8	–0.1	–12.4	40.1	44.4	41.8
6 k	–22.0	0.5	–12.3	43.0	41.3	43.6
11 k	–25.7	1.0	–13.7	34.1	54.0	40.3

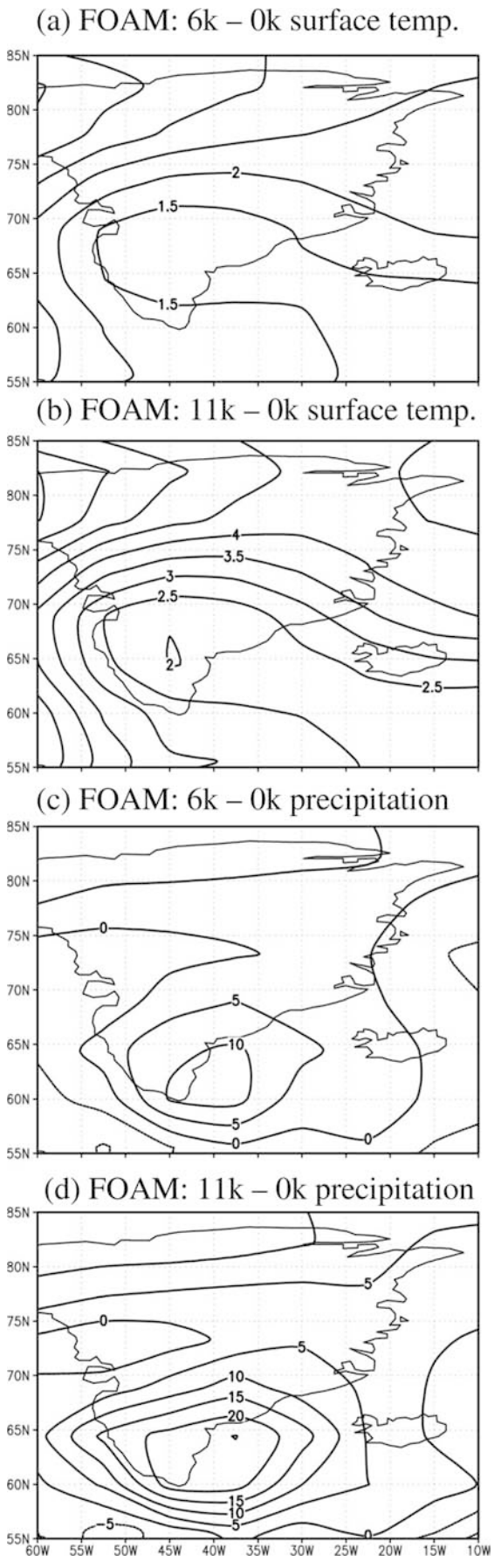

Fig. 4 Simulated July surface temperatures differences (in °C) **a** between 6 k and 0 k and **b** 11 k and 0 k as well as precipitation differences (in mm) for **c** 6 k–0 k and **d** 11 k–0 k for Greenland (from FOAM1.0). *Contour interval* is 1.5 °C for surface temperature and 5 mm for precipitation

4.1 0 k Climatology for NCEP data and model simulations

The climatological summary of the NCEP data and the model simulations for Greenland is described later.

4.1.1 Surface temperature

Present-day surface temperature for Greenland in January and July is displayed in Fig. 3 for the NCEP (a, b) and FOAM1.0 (e, f) data sets. NCEP shows the expected increase in surface temperatures from the interior (higher elevations) to the coast; in January, a sharp temperature gradient between the southern margins and the interior exists, and in July most of the coastal regions are above freezing temperature. A comparison with the July satellite derived surface temperatures (from Stroeve and Steffen 1998) reveals that the NCEP temperatures are about 5 °C warmer. Yet, as will be seen in Table 5, it will still reproduce a reasonable amount of total ablation presumably due to canceling biases in the degree-day parametrization

Both FOAM and CSM (not shown) show how elevation truncation affects surface temperature, since in January a north/south gradient is found. When calculating the area average temperature, using every grid point on land (Table 1) it is seen that FOAM1.0 simulates colder temperatures than NCEP or CSM (specially in the summer); the annual average being about 9 °C colder in FOAM than NCEP, but since NCEP is actually overestimating summer temperatures, FOAM's results are closer to observations.

4.1.2 Precipitation

Precipitation in Greenland is most intense during the winter in the southeastern region (see Fig. 3c) according to NCEP data; in the summer (Fig. 3d), it falls in the entire south region, even extending into part of central Greenland. The area average precipitation (Table 1) shows that precipitation in the summer is nearly double the value in winter.

FOAM's modeled January precipitation (Fig. 3g) fails to capture the details of the winter pattern from NCEP, since it shows only a small precipitation maxima in the southern coast of Greenland; in summer (Fig. 3h), it is more similar to NCEP although precipitation extends further inland but is less intense. The precipitation pattern in CSM (not shown) reveals the enhanced winter

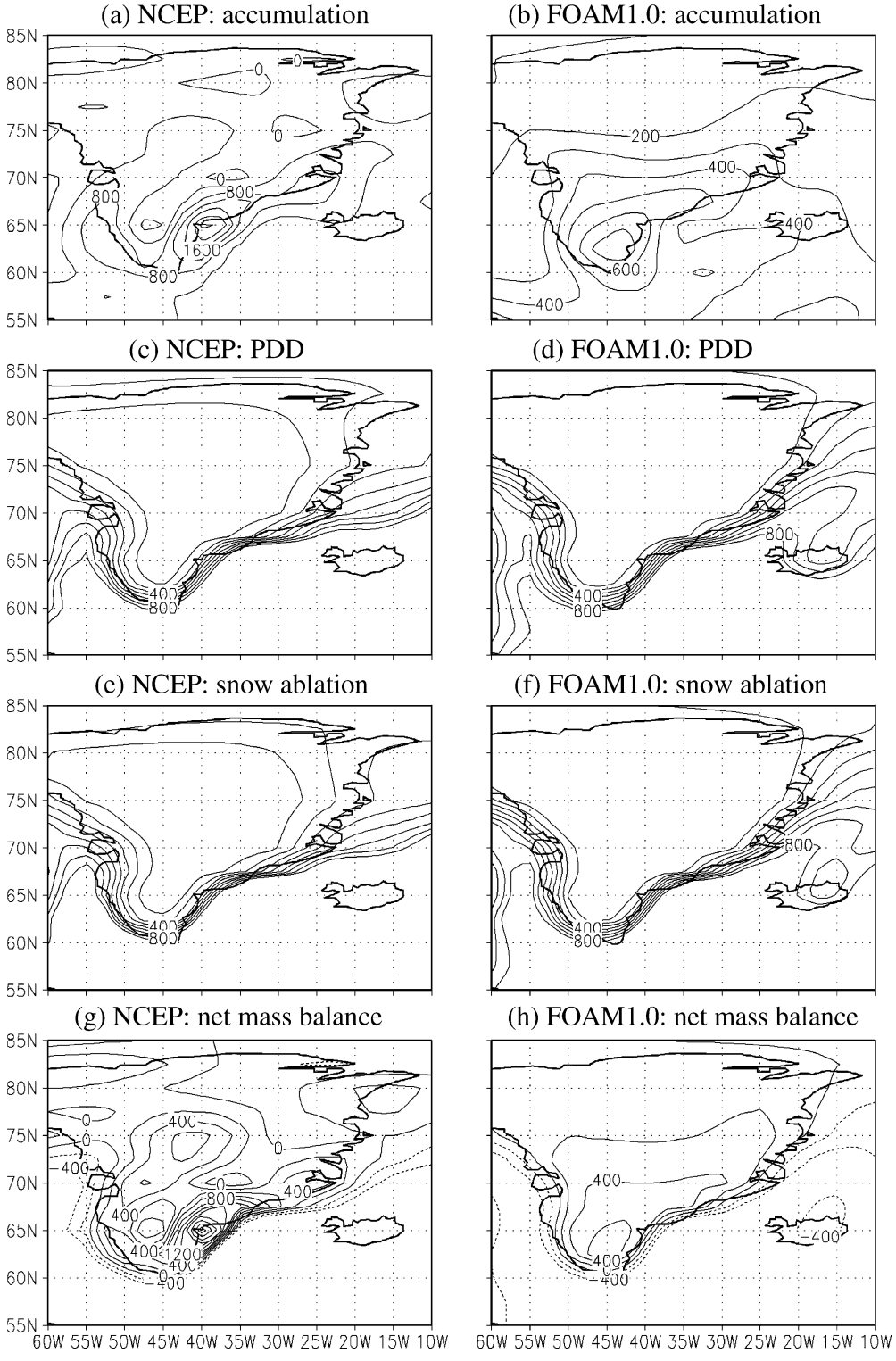

Fig. 5a, b Computed annual accumulation, **c, d** annual degree day parameter, PDD, **e, f** annual snow ablation and **g, h** annual net mass balance for Greenland, for NCEP (*left panels*) and FOAM1.0 (*right panels*). Units are °C.day for the PDD, and mm w.e/year for the remaining variables. *Contour interval* is 400 mm w.e for **a**, 100 mm w.e for **b**, 100 °C.day for **c** and **d**, 100 mm w.e for **e** and **f** and 200 mm w.e for **g** and **h**

pattern in southeastern Greenland and precipitation maximum in the south, in the summer. The area average precipitation (Table 1) shows that annually, precipitation in both models is smaller than in NCEP; FOAM reproduces the enhanced summer precipitation, CSM on the contrary, has fairly uniform precipitation throughout the year.

4.2 Past climate simulations

Since the most important season influencing the growth/decay of an ice sheet is the summer, we will hereon focus on the July results. The underlying assumption being that warmer summers cause increased snow melt versus cooler summers where the opposite occurs.

Table 3 Area averaged accumulation (in mm w.e./year), snow ablation (in mm w.e./year) and net mass balance (in mm w.e./year) for present-day conditions in Greenland. The area average was calculated with every grid point over land

0 k	Accumulation (mm w.e./year)	Snow ablation (mm w.e./year)	Net mass balance (mm w.e./year)
NCEP	306.2	60.8	245.4
FOAM1.0	297.4	6.1	291.3
CSM1.4	362.1	65.1	296.9

The area average surface temperature in Greenland (Table 2) show a progressive cooling in July, from 11 k to the present, for both models (a larger cooling of 3.6 °C for FOAM and less of a change for CSM), in agreement with the decrease in summer insolation forcing from 11 k to the present, the exception being 3 k (in FOAM) when the cooling exceeds the general cooling trend; this relative larger cooling for 3 k may be due to interannual variability.

The location of the increased early to mid Holocene summertime warmth in FOAM, for both 6 k and 11 k, is in the south (Fig. 4a, b). There is a very similar situation for CSM (not shown), in that south and southeastern Greenland was slightly warmer (0.6 °C) at 6 k compared to the present; at 11 k the entire region was at least 1 °C warmer than today.

The area average precipitation (Table 2) shows an annual decrease from 11 k to the present in FOAM; it becomes drier in both January and July towards the present with the biggest change in July (15% drier). As for CSM, it becomes wetter from 11 k to the present annually but the increase is less than 4% and may be within the interannual variability. CSM also simulates a drying from 11 k to the present (about 18%) in July.

The area with the greatest early Holocene summer precipitation increases (Fig. 4c, d) for FOAM is in south Greenland. The CSM summer precipitation differences (not shown) are in the southeastern region.

4.3 Mass balance calculations

Before calculating the net mass balance, the meteorological fields of surface temperature and precipitation had to be linearly interpolated to a common finer grid (2.5° × 2.5°). As we described in the previous section, the relatively coarse resolution of the two models truncates the topography of the Tibetan Plateau and Greenland. The NCEP topography, on the other hand, seems fairly realistic when compared with the real topography of the Tibetan Plateau and Greenland. The solution to the problem, as described in Sect. 2 (Thompson and Pollard 1997), consisted of correcting the lowest level air temperature by lowering it by a constant lapse rate multiplied by the difference between the true elevation minus the model elevation; the true elevation in this study is taken to be the NCEP topography. The lapse rate value used for Greenland was –7.0 °C/km, which represents values around Greenland in summer (Thompson and Pollard 1997). The corrected temperatures of FOAM1.0 and CSM1.4 for Greenland are in closer agreement with observations (not shown). Our corrections for past temperatures rely on the assumption that the lapse rates were the same as at present. Once the surface temperatures were corrected, the ice sheet mass balance was computed using the degree day methodology with the correction for frozen meltwater applied. It is important to mention that the sub-grid scale variations in topography, such as mountains and valleys, are not included in this study and they could, if included, lead to improvements in the mass balance results (Marshall and Clarke 1999; Walland and Simmonds 1996; Pollard and Thompson 1997a).

Table 4 Same as Table 3, for Greenland, except using past climate simulations from FOAM1.0 and CSM1.4

FOAM1.0	Accumulation (mm w.e./year)	Snow ablation (mm w.e./year)	Net mass balance (mm w.e./year)
0 k	297.4	6.1	291.3
3 k	296.0	13.0	283.0
6 k	331.1	39.8	291.3
8 k	325.7	46.5	279.2
11 k	332.3	54.3	278.0
CSM1.4			
0 k	362.1	65.1	297.0
6 k	366.3	70.8	295.5
11 k	340.3	78.4	262.0

4.3.1 Present day

Figure 5a–h summarizes the mass balance results for Greenland from NCEP and FOAM. The maximum accumulation in NCEP (Fig. 5a) occurs in the southeastern sector of Greenland due to orographic uplift by onshore winter flow (Ohmura and Reeh 1991; Pollard et al. 2000); minimum accumulation occurs in the central and northern regions. These results agree fairly well with actual data from Ohmura and Reeh (1991) and Pollard et al. (2000). The annual degree day factor (Fig. 5c) shows a sharp increase from the interior towards the coast and, since ablation is directly related to it, the ablation (Fig. 5e) is confined mainly to the periphery, which according to Pollard et al. (2000) is an indication of the strong control of topography and lapse rate. The net annual mass balance (Fig. 5g) has a highest positive value of around 1600 mm w.e./year in the southeast which reflects the presence of a local topographic plateau near high bedrock (Pollard et al. 2000).

Both FOAM (Fig. 5b, d, f and h) and CSM (not shown) patterns for accumulation, degree day parameter and ablation agree well with those from NCEP with the maximum accumulation in the southeast (Fig. 5a) and the ablation (Fig. 5f) located in the coastal areas (where the degree day parameter is highest , Fig. 5d). Therefore, as expected, the net annual mass balance (Fig. 5h) is

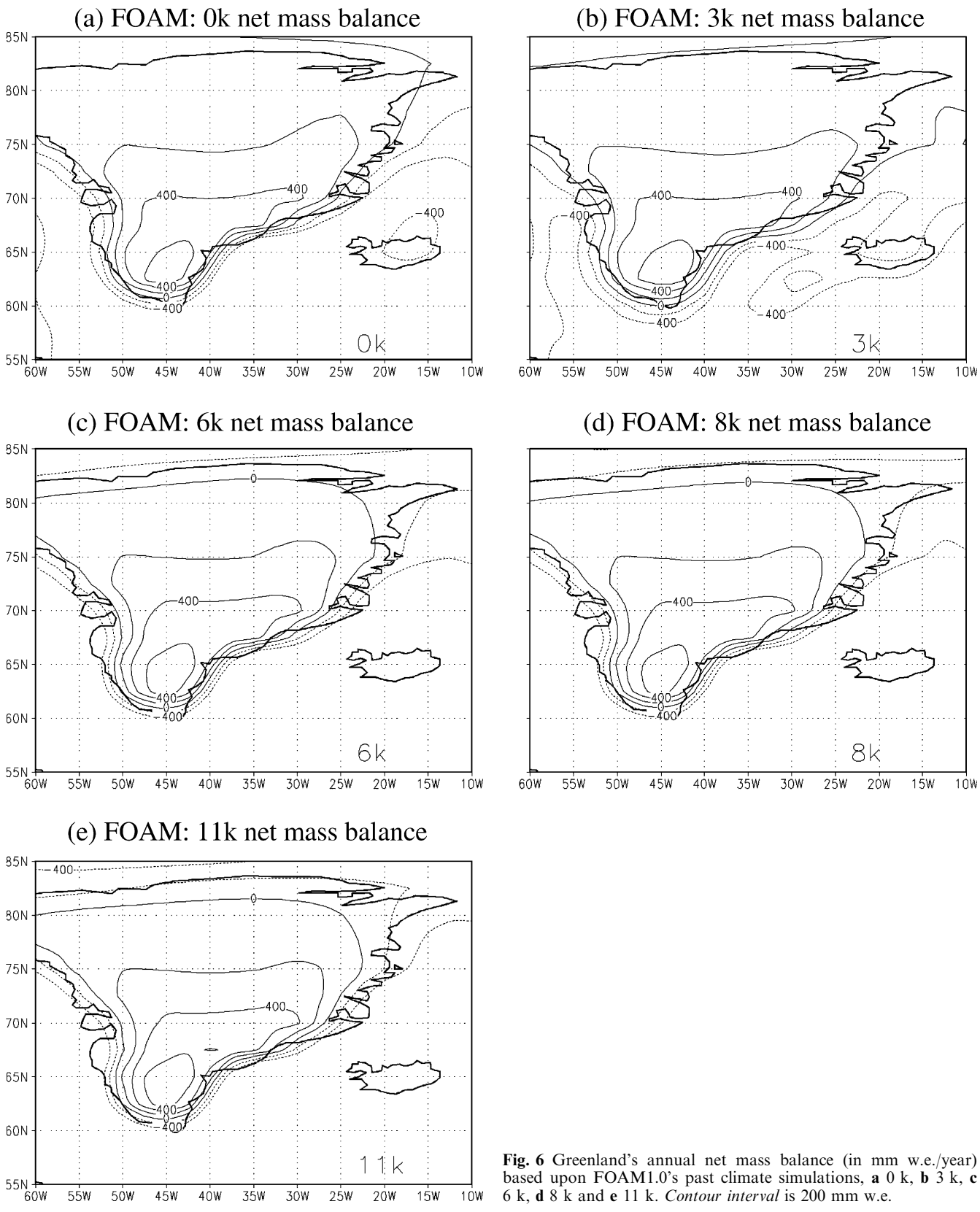

Fig. 6 Greenland's annual net mass balance (in mm w.e./year) based upon FOAM1.0's past climate simulations, **a** 0 k, **b** 3 k, **c** 6 k, **d** 8 k and **e** 11 k. *Contour interval* is 200 mm w.e.

positive in both models with highest values in the southeastern region and decreasing values inland and to the north.

The area average (for all land grid points) mass balance variables (Table 3) show that the accumulation rates from the three different datasets are rather close,

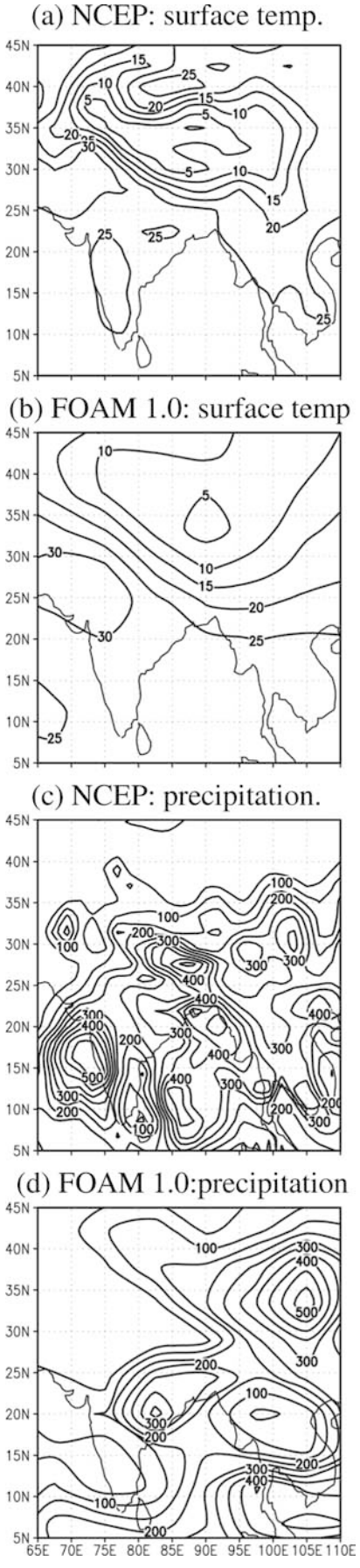

◀

Fig. 7 July present-day surface temperature (in °C) **a** for NCEP and **b** FOAM1.0 as well as precipitation (in mm) for **c** NCEP and **d** FOAM1.0 for the Tibetan Plateau. *Contour interval* is 5 °C for surface temperature and 50 mm for precipitation, in both datasets

with CSM giving the highest estimate. Snow ablation is rather small for FOAM, a likely consequence of the simulated low surface temperatures, (described in the previous section) and both NCEP and CSM give larger and rather similar estimates. These results agree well with the conclusions from Ohmura and Reeh (1997) and Pollard et al. (2000). The net mass balances for the three datasets range from about 250 to 300 mm w.e./year and are somewhat higher than the value of 130 mm w.e./year obtained by Thompson and Pollard (1997b) using version 2 of GENESIS but fall within the range (–800 to +600 mm w.e./year) of the 17 GCM's final mass balances used in the study of Pollard et al. (2000).

4.3.2 Past climate simulations

The results of the area averaged mass balance calculations using the past surface temperature (corrected) and precipitation (Table 4) shows that accumulation has slightly decreased in FOAM from the beginning of the Holocene to present ($\backsim$35 mm w.e./year), although the decrease is not monotonic. CSM on the other hand yields a small increased accumulation from 11 k to 0 k ($\backsim$22 mm w.e./year). Ablation decreases from 11 k to present in both models, with FOAM experiencing the largest decrease ($\backsim$48 mm w.e./year). These results are consistent with the 6 k results from Pollard and PMIP Participating Groups (2000). The net mass balance trend was slightly positive from 11 k to 0 k in both models, with CSM yielding the largest increase (13%). Figure 6a–e displays the spatial contours of the net mass balance for FOAM (CSM is not shown) confirming that the spatial pattern of Greenland's simulated mass balance has been fairly constant since the beginning of the Holocene.

5 Mass balance calculations for the Tibetan Plateau

The following section describes all the results for the Tibetan Plateau. Because the present-day mass balance results for Greenland agree fairly well with the results from previous studies (see Sect. 2), it provided us some confidence in using the same approach for the Tibetan Plateau.

5.1 0 k Climatology for NCEP data and model simulations

The climatological summary of the NCEP data and the model simulations are described.

Table 5 Area average surface temperature (in °C) and monthly cumulative precipitation (in mm) for present-day Tibetan Plateau, for NCEP, FOAM1.0 and CSM1.4 The area average was calculated for every grid point above 2000 m. In parenthesis are displayed the lapse rate corrected surface temperatures (in °C) using the lapse rate value of 5 °C/km

0 k	Surface temperature(°C)			Monthly cumulative precipitation(mm)		
	January	July	Annual	January	July	Annual
NCEP	–11.7	10.1	–0.6	30.7	139.5	69.0
FOAM1.0	–15.9 (–17.0)	9.5(8.1)	–1.6(–3.0)	29.7	147.8	74.6
CSM1.4	–9.7(–12.0)	14.2(12.2)	3.0(1.0)	35.2	163.6	85.7

5.1.1 Surface temperature

The surface temperature pattern for NCEP data in the Tibetan Plateau region shows that in July (Fig. 7a) the highest elevations are only slightly above freezing whereas in January (not shown) most of the plateau experiences much below freezing temperatures. Both FOAM's (Fig. 7c) and CSM's (not shown) surface temperature patterns have a smaller dependence on surface elevation than NCEP, which is expected due to the high topographic resolution in NCEP. These differences decrease when model temperatures are corrected for elevation bias (see Sect. 4).

The surface temperature, averaged for every grid point above 2000 m for the different datasets (Table 5) shows that FOAM simulates colder temperatures than the NCEP climatology. CSM simulates somewhat warmer temperatures than the NCEP climatology.

5.1.2 Precipitation

Precipitation patterns for NCEP data (Fig. 7b) and for the FOAM simulation (Fig. 7d) in July are in fair agreement and illustrate the strong Asian summer monsoon. In January (not shown) most of the heavy precipitation is located over the ocean south of 10°N, but as the season progresses and the monsoon arrives, heavy precipitation moves further north and reaches the maximum latitude of 35°N in July only to start retreating in August (not shown). The band of precipitation enters the mainland first from the southeast. Regional differences do occur in both FOAM and CSM, particularly in Western India where the monsoon is underestimated and eastern Asia where it is overestimated in both models. The area average precipitation on the Tibetan Plateau (Table 5) indicates the large precipitation during July. Both models overestimate precipitation compared to NCEP, particularly CSM.

5.1.3 Past climate simulations

The area average temperature in July (Table 6) decreased from 11 k to the present in both models, with the largest decrease occurring in FOAM (from 14 °C at 11 k to 9.5 °C at present); in January the temperature increased in both models, the exceptions being the 3 k values for FOAM and the 6 k values in CSM. In both case, the trends agree well with the trends in the insolation forcing. The surface pattern differences in the Tibetan Plateau, for FOAM (Fig. 8a) in July, for 6 k, show that most of the area north of 30°N was 1 °C warmer than at 0 k and, at highest altitudes, 2 °C warmer. At 11 k, the July anomalies (Fig. 8b) are also positive and higher than at 6 k (up to 6 °C difference). CSM's temperature difference pattern (not shown), although regionally different from FOAM's, shows similar sign anomalies in January and July, the exception being 6 k where negative anomalies were found in the summer (see also Table 6).

The average precipitation in the Tibetan Plateau above 2000 m (Table 6), indicates that July became drier towards the present (about 20% less rain at 0 k than 11 k) and that January became wetter (about 25%) from the early Holocene to the present; these trends occurred in both models. The annual average precipitation decreased for both models indicating the dominance of summer precipitation. Figure 8c and 8d illustrate the precipitation difference pattern for FOAM in July (CSM is very similar) and clearly show the positive rainfall anomalies for both 6 k and 11 k, located on the southern and eastern sides of the plateau.

5.2 Mass Balance calculations

The surface temperature was lapse-rate corrected, just as in the case of Greenland, however the correction was much larger owing to the larger topographic bias for the Tibetan Plateau (see Fig. 1a–c). A lapse rate of 5 °C/km was used for the region above the Tibetan Plateau based upon calculations using the NCEP reanalysis data; these calculations showed values of 5 to 6 °C/km, depending upon the season. The area average results of the correction are summarized in Table 5 in parenthesis and upon comparison with the uncorrected values, we see that average temperatures were lowered by $\backsim$ 1.5 °C for FOAM and $\backsim$ 2.0 °C for CSM. Figure 9a, b displays the uncorrected versus corrected July surface temperature and show a definite

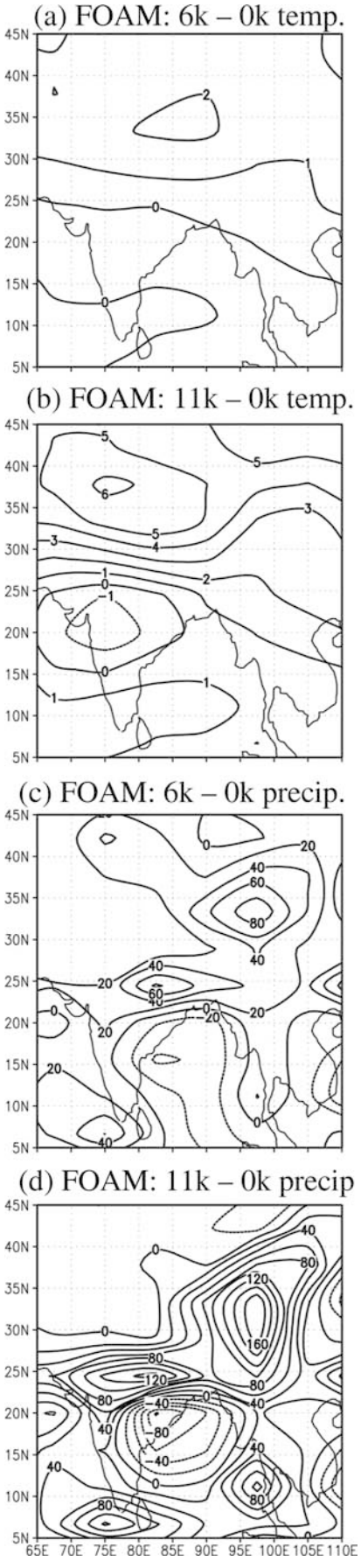

Fig. 8 Simulated July surface temperatures differences (in °C) **a** between 6 k and 0 k and **b** 11 k and 0 k and precipitation differences (in mm) **c** for 6 k–0 k and **d** 11 k–0 k for the Tibetan Plateau (from FOAM1.0). *Contour interval* is 1 °C for surface temperature and 20 mm for precipitation

improvement since the corrected temperature is dependent on the topography.

5.2.1 *Present day*

The annual accumulation on the Tibetan Plateau occurs in the highest altitudes (above 4 km) and the highest value of 600 mm w.e./year is found to the east of the highest elevations in the NCEP dataset (Fig. 10a). The positive degree day parameter increases with lowering altitude (Fig. 10c) as does the snow ablation (Fig. 10e). The net mass balance (Fig. 10g) is negative for most of the Plateau, the exception being two small areas in the central part where positive values are found (from +100 to +200 mm w.e./year). This result seems to reproduce reasonably well the present situation, since only small areas nowadays are glaciated in the Tibetan Plateau and their exact characteristics are far too small to be captured in detail by the coarse model resolution.

The accumulation computed from FOAM (with the temperature correction) is slightly higher than in NCEP (Fig. 10b) and extends farther north and east. The maximum accumulation is still found east of the highest elevations but it reaches the value of 1000 mm w.e./year. The degree day parameter and snow ablation is similar to NCEP (Fig. 10d, f) and the net mass balance (Fig. 10h) displays a small region (which includes the highest elevation) where the mass balance is positive, between 250 and 500 mm w.e./year, which is a consequence of the higher modeled accumulation values. Everywhere else, the net mass balance is negative. Overall, agreement between NCEP and the model simulations is fairly good.

CSM1.4 present-day accumulation (not shown) is comparable to NCEP's and so is the snow ablation (not shown). As a result, there is a negative mass balance for almost the entire Tibetan Plateau, but again with a small positive mass balance at the highest elevation.

Table 7 summarizes the area average results and shows that FOAM accumulates the most snow and that CSM melts the most snow. All three datasets yield a negative mass balance averaged over the area above 2000 m, and NCEP values lie somewhat between those from FOAM and CSM.

5.2.2 *Past climate simulations*

The area averaged results for the mass balance calculations with the past climate datasets are shown in

Table 6 Same as Table 5, for the Tibetan Plateau, except for past climate simulations from FOAM1.0 and CSM1.4

FOAM1.0	Surface temperature(°C)			Monthly cumulative precipitation(mm)		
	January	July	Annual	January	July	Annual
0 k	–15.9	9.5	–1.6	29.7	147.8	74.6
3 k	–17.4	8.2	–3.3	25.0	144.6	71.2
6 k	–16.6	11.2	–1.6	24.4	177.9	77.8
8 k	–17.1	12.4	–1.7	23.1	188.2	79.4
11 k	–17.7	14.0	–1.4	23.8	193.3	81.8
CSM1.4						
0 k	–9.7	14.2	3.0	35.2	163.6	85.7
6 k	–15.0	12.5	–0.5	34.6	177.6	89.6
11 k	–14.4	15.6	1.1	27.7	207.6	95.0

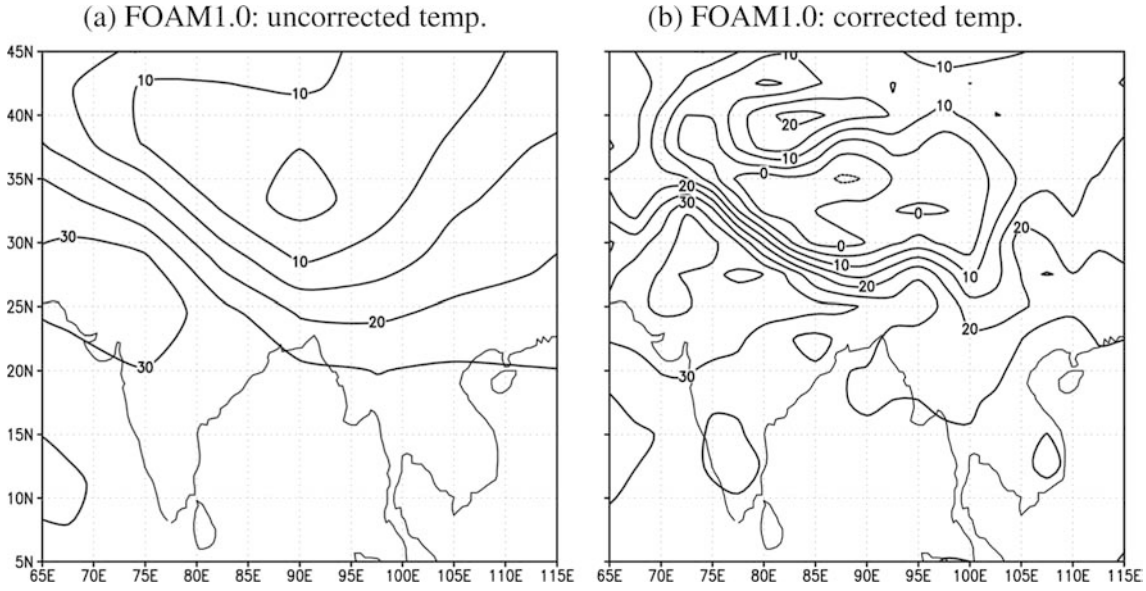

Fig. 9 Present-day lapse rate uncorrected **a** versus corrected **b** July surface temperatures (in °C) for the Tibetan Plateau, for FOAM1.0. *Contour interval* is 5 °C

Table 8. The accumulation in FOAM increased from 11 k to the present (by 12%) and ablation decreased by an even larger percentage (19%) owing to the trend towards cooler summers. Therefore, the net mass balance became less negative from 11 k to the present (a reduction of 26%), owing mainly to the decreased ablation which is in turn related the significant lowering in summer temperature (see Table 4 for the July surface temperature). The trend in the CSM results is difficult to assess due to the lack of the 3 k and 8 k datasets; nevertheless the tendency is for a slightly more negative mass balance at the present compared to 11 k (a change of 6%) due to decreased accumulation and increased ablation. Overall, the changes in FOAM are larger than those in CSM1.4 and one factor that might possibly account for this difference is that the July temperature lowering in CSM between 11 k and present was consistently less than the lowering in FOAM. Figure 11a–e shows that the area with positive mass balance in FOAM expands from 11 k to 0 k; the opposite occurs with CSM (not shown). The important result in FOAM is that at 11 k most of the Tibetan Plateau is in negative balance, therefore unable to sustain any ice sheets, but the area of potential ice sheets increases with time; this result partly fits the observations, especially for the Dasuopu ice cap which dates back only to the Holocene, 6000 to 8000 year BP, as mentioned earlier (Thompson et al. 2000).

6 Conclusions and suggestions for additional work

Using the three sets of data, one from NCEP reanalysis, and two from GCMs (FOAM1.0 and CSM1.4), ice-sheet mass balance calculations were made for Greenland and the Tibetan Plateau for the present day, and for past simulations, under the insolation forcings at 3 k, 6 k, 8 k and 11 k. Even though several studies on the present-

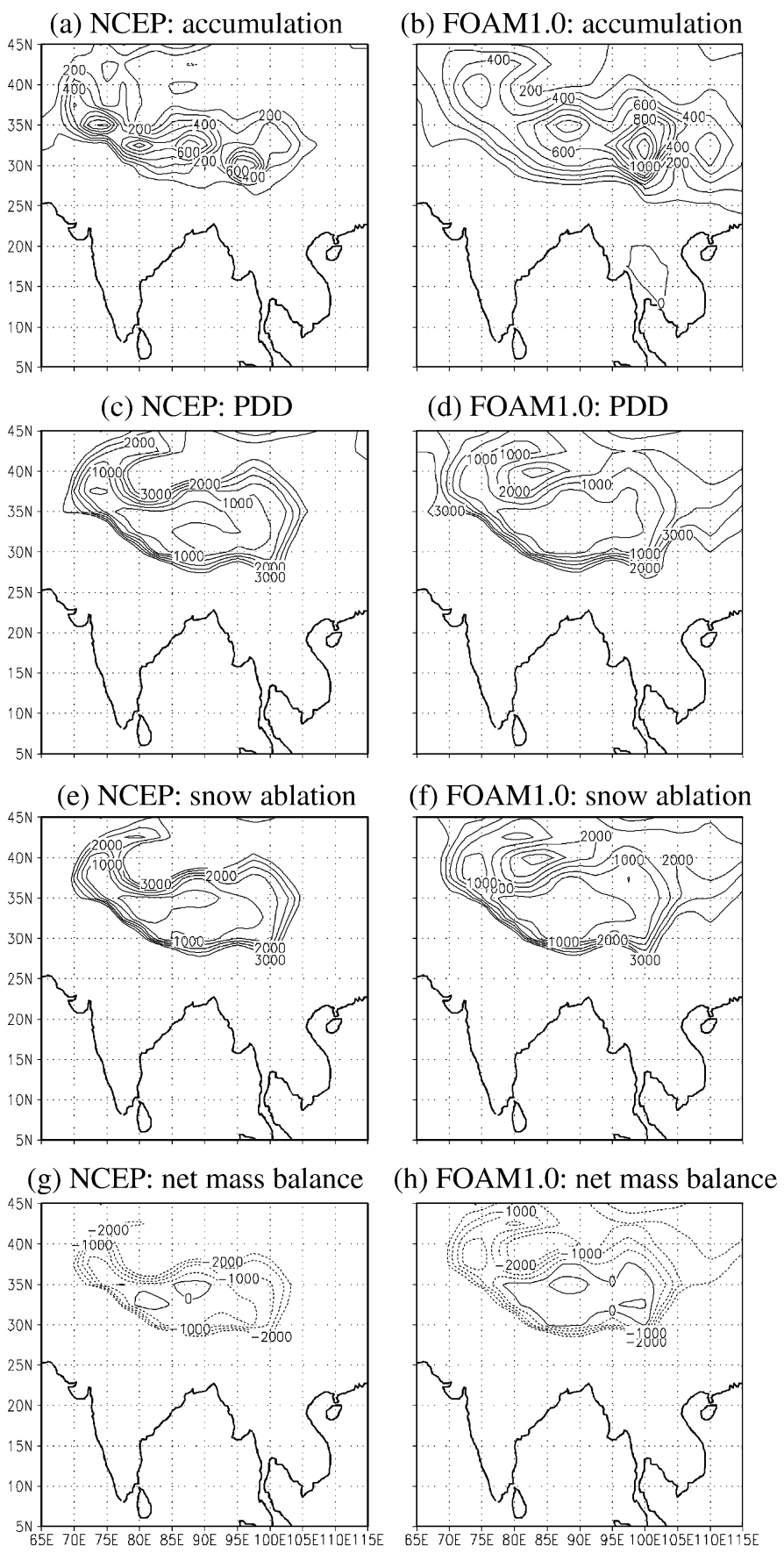

Fig. 10 a, b Computed annual accumulation **c, d**, annual degree day parameter, PDD, **e, f** annual snow ablation and **g, h** annual net mass balance for the Tibetan Plateau, for NCEP (*left panels*) and FOAM1.0 (*right panels*). Units are °C.day for the PDD, and mm w.e/year for the remaining variables. The *contour interval* for **a** and **b** is 100 mm w.e., for **c** and **d** is 500 °C.day and for **e**–**h** is 500 mm w.e.

Table 7 Area averaged accumulation (in mm w.e./year), snow ablation (in mm w.e./year) and net mass balance (in mm w.e./year) for present day conditions for the Tibetan Plateau. The area average was calculated using every grid point above 2000 m

0 k	Accumulation (mm w.e./year)	Snow ablation (mm w.e./year)	Net mass balance (mm w.e./year)
NCEP	247.7	1920.1	–1672.3
FOAM1.0	440.6	1600.4	–1159.8
CSM1.4	341.3	2326.3	–1985.0

Table 8 Same as Table 7, for the Tibetan Plateau, except using past climate simulations from FOAM1.0 and CSM1.4

FOAM1.0	Accumulation (mm w.e./year)	Snow ablation (mm w.e./year)	Net mass balance (mm w.e./year)
0 k	440.6	1600.4	–1159.8
3 k	455.8	1350.7	–894.9
6 k	409.1	1753.0	–1344.0
8 k	402.7	1823.8	–1421.1
11 k	391.6	1957.9	–1566.3
CSM1.4			
0 k	341.3	2326.3	–1985.0
6 k	431.4	1777.3	–1345.9
11 k	367.3	2230.7	–1863.4

day Greenland mass balance exist (observational as well as modeled), there are none (to our knowledge) on the Tibetan Plateau.

One of the several problems in simulating realistic mass balance on ice sheets is that the relatively coarse resolution of GCM's is not able to capture the observed topography, therefore the solution was to interpolate the meteorological fields to a finer grid, a $2.5° \times 2.5°$ in this case, and then apply a lapse rate temperature correction to the surface temperature to account for the topographic bias.

A degree day model was used to estimate ablation and accumulation based upon monthly precipitation and temperature. The resulting calculations for Greenland agreed quite well with the results from previous work in that most accumulation occurs in the southeast and ablation was confined mainly to the coastal regions. As to the present day mass balance, a value of 245.4 mm w.e./year was obtained for NCEP; while values of 291 mm w.e./year were obtained for FOAM and 197 mm w.e./year for CSM. The past simulations revealed that the general trend in both models was toward a slightly more positive mass balance from the beginning of the Holocene (11 k) to the present (5% to 13% estimates for FOAM and CSM, respectively).

The Tibetan Plateau ice sheet mass balance results were quite different from those of Greenland. The present area average mass balance for the Tibetan Plateau is negative, ranging from the calculated values of –1160 mm w.e./year for FOAM1.0 to –1985 mm w.e./year for CSM1.4, even though locally small high-altitude areas had a positive mass balance, i.e., areas where ice sheets could develop. Comparing the early Holocene simulations with the present simulation for FOAM, accumulation increased from 11 k to 0 k, but there was a larger decrease in ablation (related to a significant drop in summer surface temperatures which are consistent with the orbitally- caused increasingly cooler summers towards the present). Consequently, the net mass balance became less negative by approximately 26%. The net mass balance for CSM, on the other hand, became more negative (but the change was small, only 6%) most probably due to the smaller cooling of summer temperatures from 11 k to 0 k in CSM, compared to FOAM. Further work is needed to completely understand the differences between the two models, including analysis of intermediate time experiments for CSM at 3 k and 8 k so as to calculate more reliable trends.

We conclude, based primarily upon the more complete sequence of FOAM results, that in the early Holocene the Tibetan Plateau had relatively large areas of negative mass balance which would have been unlikely to fulfill the necessary climatic conditions to grow ice sheets, but that the increasingly lower summer temperatures towards the present could have allowed small ice sheets to grow over a larger region, provided, of course, that the appropriate conditions prevailed at the small scale. This result of our simulation studies is potentially consistent with some observations, in particular, the observed development of the Dasuopu and other ice sheets in the Holocene, particularly in the more southern and central portions of the Plateau.

Finally, in terms of future work, the use of a finer spatial resolution grid should be considered in order to include even smaller-scale topographic factors. Moreover, a different mass balance calculation method, such as an energy balance approach, could be examined as an alternative to the simplified degree-day approach used here. Furthermore, continued improvement of models will hopefully lead to reductions in the temperature and precipitation biases noted here. It would also be desirable to increase the length of the runs to ensure equilibrium solutions. We were unable to resolve satisfactorily the cause of the different sensitivity of the mass balance calculations of the two models, and that too would be a topic for continuing work.

Acknowledgements The authors would like to thank Shawn Marshall for his valuable advice, and Roderik Van de Wal help at various stages. Bette Otto-Bliesner provided the CSM1.4 data and Pat Behling and Sara Rauscher provided computing assistance. The comments of the reviewers, including David Pollard, led to substantial improvements. Thank you. Funding for this work was provided by the National Science Foundation (Climate Dynamics and Earth System History Programs, Grants NSF-ATM 0002937 and NSF-ATM 9905285) and the Portuguese Foundation for Science and Technology (Grant: SFRH/BD/788/2000). This is CCR publication number 834.

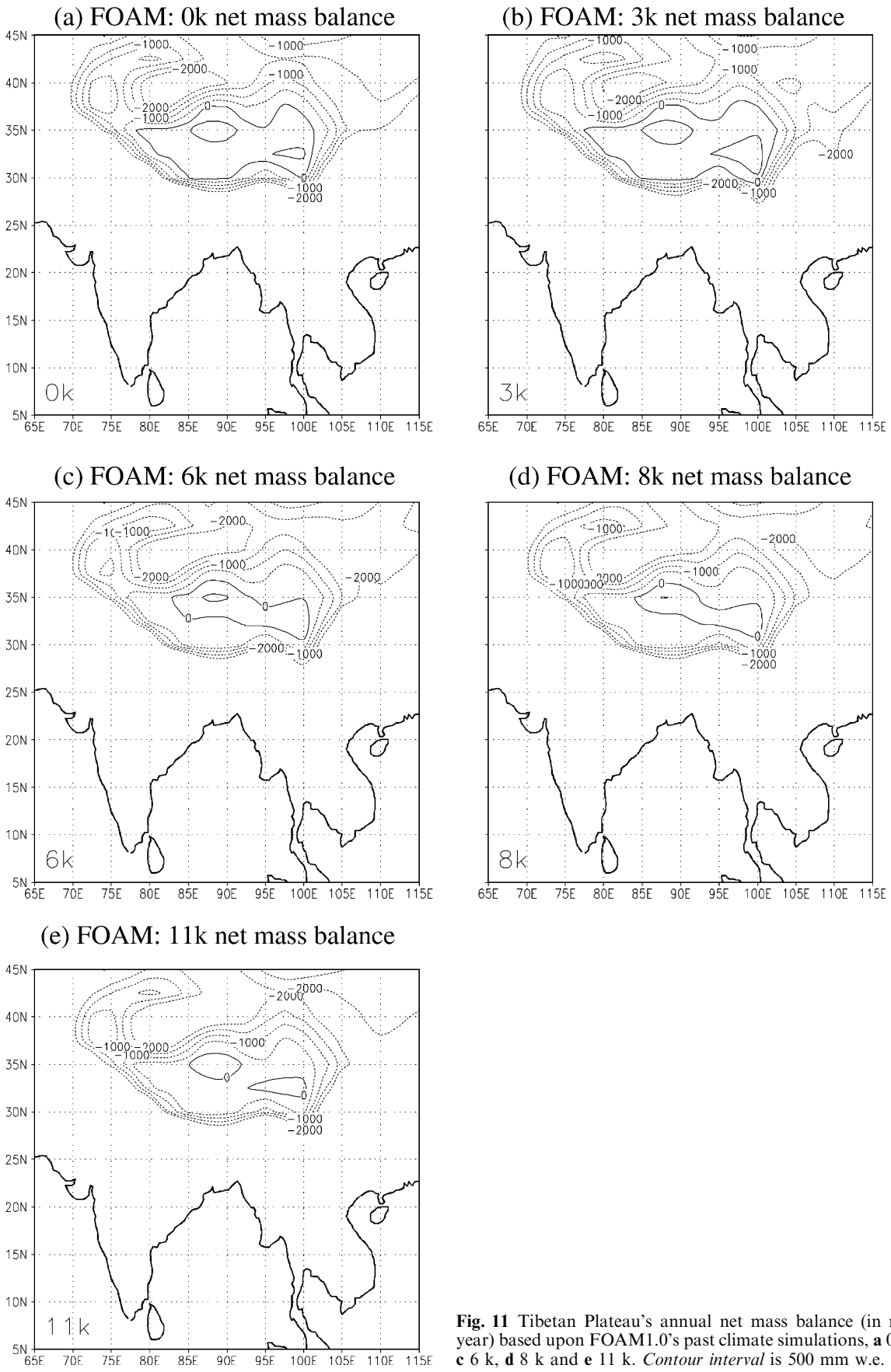

Fig. 11 Tibetan Plateau's annual net mass balance (in mm w.e./year) based upon FOAM1.0's past climate simulations, **a** 0 k, **b** 3 k, **c** 6 k, **d** 8 k and **e** 11 k. *Contour interval* is 500 mm w.e.

References

Abdalati W, Steffen K (1997) Snowmelt on the Greenland ice sheet as derived from passive microwave satellite data. J Clim 10: 165–175

Braithwaite RJ (1996) Models of ice-atmosphere interactions for the Greenland ice sheet. Ann Glaciol 23: 149–153

Christner BC, Mosley-Thompson E, Thompson LG, Reeve JN (2003) Bacterial recovery from ancient glacial ice. Environ Microbiol 5(5): 433–436

Gent PR, Bryan FO, Danabasoglu G, Doney SC, Holland WR, Large WG, McWilliams JC (1998) The NCAR climate system model global ocean component. J Clim 11: 1287–1306

Huybrechts P, Letreguilly A, Reeh N (1991) The Greenland ice sheet and greenhouse warming. Palaeogeogr Palaeoclimatol Palaeoecol 89: 399–412

Imbrie J, Imbrie KP (1979) Ice ages, solving the mystery. Harvard University Press, Harvard, Cambridge, Mass USA pp 224

IPCC (2001) Climate change 2001: synthesis report. In: Watson RT and the Core Writing Team (eds.) A Contribution of Working Groups I, II and III to the Third Assessment Report of the Integovernmental Panel on Climate Change. Cambridge University Press, Cambridge, UK pp 398

Jacob RL (1997) Low frequency variability in a simulated atmosphere ocean system. Ph.D. Thesis, University of Wisconsin, Madison, USA

Kiehl JT, Hack JJ, Bonan GB, Boville BA, Williamson DL, Rasch PJ (1998) The national center for atmospheric research community climate model:CCM3. J Clim 11: 1131–1149

Liu K-B, Yao Z, Thompson LG (1998) A pollen record of Holocene climatic changes from the Dunde ice cap, Qinghai-Tibetan Plateau. Geology 26(2): 135–138

Liu Z, Otto-Bliesner B, Kutzbach J, Li L, Shields C (2004) Coupled climate simulations of the evolution of global monsoons in the Holocene. J Clim (in press)

Liu Z, Brady E, Lynch-Stieglitz J (2003) Global ocean response to orbital forcing in the Holocene. Paleoceanography 18(2): 19–1–19–20

Marshall SJ, Clarke GKC (1999) Ice sheet inception: subgrid hypsometric parametrization of mass balance in an ice sheet model. Clim Dyn 15: 533–550

Marshall SJ, James TS, Clarke GKC (2002) North American ice sheet reconstructions at the Last Glacial Maximum. Q Sci Rev 21: 175–192

Ohmura A, Reeh N (1991) New precipitation and accumulation maps for Greenland. J.Glaciol 37: 140–148

Ohmura A, Wild M, Bengtsson L (1996) A possible change in mass balance of Greenland and Antarctic ice sheets in the coming century. J Clim 9: 2124–2135

Pollard D, Thompson SL (1997a) Driving a high-resolution dynamic ice-sheet model with GCM climate: ice-sheet initiation at 116,000 BP. Ann Glaciol 25: 296–304

Pollard D, Thompson SL (1997b) Climate and ice sheet mass balance at the Last Glacial Maximum from the GENESIS Version 2 Global Climate Model. Quat Sci Rev 16: 841–863

Pollard D, PMIP Participating Groups (2000) Comparisons of ice-sheet surface mass budgets from Paleoclimate Modeling Intercomparison Project (PMIP) simulations. Global Planet Change 24: 79–106

Shin S-I, Liu Z, Otto-Bliesner B, Brady EC, Kutzbach JE, Harrison SP (2003) A simulation of the Last Glacial Maximum climate using the NCAR-CCSM. Clim Dyn 20: 127–15

Stroeve J, Steffen K (1998) Variability of AVHRR-derived clear-sky surface temperature over the Greenland Ice Sheet. J Appl Meteorol 31: 23–31

Stroeve J, Nolin A, Steffen K (1997) Comparison of a AVHRR-derived and in situ surface albedo over the Greenland Ice Sheet. Remote Sensing Environ 62: 262–276

Thompson SL, Pollard D (1997) Greenland and Antarctic mass balances for present and doubled atmospheric CO_2 from the GENESIS Version-2 Global Climate model. J Clim 10: 871–900

Thompson LG, Yao T, Davis ME, Henderson KA, Mosley-Thompson E, Lin P-N, Beer J, Synal H-A, Cole-Dai J, Bolzan JF (1997) Tropical climate instability: the last glacial cycle from a Qinghai-Tibetan ice core. Sci 276: 1821–1825

Thompson LG, Mosley-Thompson E, Davis ME, Bolzan JF, Dai J, Yao T, Gundestrup N, Wu X, Klein L, Xie Z (1989) Holocene-late Pleistocene climatic ice core records from Qinghai-Tibetan Plateau. Sci 246(4929): 474–478

Thompson LG, Yao T, Mosley-Thompson E, Davis ME, Henderson KA, Lin P-N (2000) A high-resolution millennial record of the South Asian monsoon from Himalayan ice cores. Sci 289: 1916–1919

Walland DJ, Simmonds I (1996) Sub-grid scale topography and the simulation of Northern Hemisphere snow cover. Int J Clim 16: 961–982

Van de Wal RSW (1996) Mass-balance modeling of the Greenland ice sheet: a comparison of an energy-balance and a degree day model. Ann Glaciol 23: 36–45

Van de Wal RSW, Wild M, De Wolde J (2001) Short-term volume changes of the Greenland ice sheet in response to doubled CO_2 conditions. Tellus 53(B): 94–102

Wild M, Calanca P, Scherrer SC, Ohmura A (2003) Effects of polar ice sheets on global sea level in high-resolution greenhouse scenarios. J Geophys Res 108(D5): 5-1–5-10